Aust. J. Phys., 1986, **39**, 809–27

Photoionisation and Auger Electron Emission from the Lithium Molecule: Calculations using Multicentre Numerical Continuum Functions*

F. P. Larkins[A] *and J. A. Richards*[B]

[A] Department of Chemistry, University of Tasmania, P.O. Box 252C, Hobart, Tas. 7001.
[B] Department of Chemistry, Monash University, Clayton, Vic. 3168.

Abstract

A numerical method has been used for the generation of molecular continuum wavefunctions at the relaxed Hartree–Fock level associated with the photoionisation of the lithium molecule. Exchange between the continuum electron and the ion core is included, but L coupling is neglected. Cross sections for core and valence shell photoionisation have been calculated from threshold to 6·0 a.u. The results differ significantly in detail from previous multiple scattering calculations. Continuum phase shifts and the asymmetry parameters for the various processes are also reported. The molecular cross section values are compared with atomic cross sections calculated at the relaxed Hartree–Fock level. The Li_2 molecular Auger transition rates are also calculated from first principles using the appropriate two-centre continuum functions. The results provide a basis for the reinterpretation of recent experimental findings of photoemission data for the lithium vapour system.

1. Introduction

A major challenge in the calculation of molecular photoionisation cross sections and the associated angular distribution parameters is to describe adequately the final continuum state involving the ejected photoelectron. A range of methods has been proposed to address this problem. Many are approximate in nature and do not require the explicit evaluation of continuum wavefunctions. Such methods do not provide a basis for a theoretical description of photoelectron angular distributions, or of Auger electron emission. A fully numerical method of evaluating molecular continuum functions has been reported recently (Richards and Larkins 1984, 1986). It has been previously applied to calculate photoionisation phenomena associated with the hydrogen molecule and the hydrogen molecule ion. In this paper the numerical method has been used to calculate continuum functions for the determination of photoionisation cross sections, angular distribution parameters and Auger transition probabilities associated with the lithium molecule. The photoionisation findings are compared with atomic cross sections. The work provides a basis for the reinterpretation of the photoemission data of Krummacher *et al.* (1982) and Gerard (1984).

Photoionisation of the lithium dimer Li_2 is of fundamental importance. Theoretically Li_2 is the electronically simplest stable homonuclear diatomic molecule after H_2.

* Paper presented at the Specialist Workshop on Excited and Ionised States of Atoms and Molecules, Strathgordon, Tasmania, 3–7 February 1986.

0004-9506/86/050809$02.00

It has a large internuclear equilibrium separation of 5·052 a.u. The ground state electronic structure Li_2 $1\sigma_g^2\,1\sigma_u^2\,2\sigma_g^2\,(^1\Sigma_g^+)$ contains both core and valence electrons. Previous investigations of the electronic properties of Li_2 have tended to concentrate on bound state calculations of ground and excited Li_2, and valence hole states of Li_2^+, due to the interest in Li_2 for laser use (Harris 1980; Hyman and Mani 1977). The most important theoretical contribution has been the series of multiconfiguration self-consistent field (MCSCF) studies by Konowalow and coworkers (Konowalow and Fish 1984; and references therein). Reviews of this area are given by Schmidt-Mink *et al.* (1985) and Hessel and Vidal (1979). The present work on Li_2 continuum processes complements the existing bound state work.

There has been only one previous calculation of either core or valence photoionisation in Li_2, namely, the multiple scattering calculation of Davenport *et al.* (1983). The corresponding photoionisation of atomic Li has been studied more extensively. Both core (Amusia *et al.* 1976; Larkins *et al.* 1981, 1986; de Alti *et al.* 1983) and valence (McDowell and Chang 1969; Chang and Poe 1975; Bhatia *et al.* 1975; Tiwari *et al.* 1977; Sukumar and Kulander 1978) studies have been reported.

The Li_2 molecule is also the simplest diatomic molecule in which Auger emission processes are significant. Although little is known experimentally or theoretically about the Li_2 Auger processes, Li_2 is a convenient system on which to test the two-dimensional numerical continuum method. Calculations of the Auger transition rates are presented herein.

2. Theory

(a) Photoionisation cross section

The cross section for photoionisation of a system in initial state 'i' by an unpolarised photon beam of energy $h\nu$, ejecting a photoelectron of energy ϵ, leaving the system in final state 'f' is given by

$$\sigma(\epsilon) = \frac{4\pi^2 \alpha a_0^2}{3 g_i}(\epsilon + I_{if})|M_{if}|^2, \tag{1}$$

where α is the fine-structure constant, a_0 is the Bohr radius and g_i is the statistical weight of the initial discrete state. The ionisation energy I_{if} and the photoelectron energy ϵ are in atomic units, and σ is in units of Mb (10^{-18} cm^2). Within the dipole approximation the transition moment M_{if} is given by

$$M_{if} = \langle \Psi^f_n | \sum_j d_j | \Psi^i_0 \rangle, \tag{2}$$

where Ψ^i_0 and Ψ^f_n are the total initial- and final-state functions, respectively, for the N-electron system and d_j is the one-electron dipole operator. If the wavefunctions Ψ^i_0 and Ψ^f_n are exact, there are two equivalent forms of the dipole operator: $d_j = r_j$ (length form) and $d_j = \nabla_j/(E^f_n - E^i_0)$ (velocity form). When non-exact wavefunctions are used in practice, the forms are no longer formally equivalent. For diagram photoionisation processes, especially those involving the lowest member of a state manifold, it can be shown (Manson 1976; Richards and Larkins 1983) that generally no one form is to be preferred. In practice, both forms should be evaluated,

since the agreement between the forms provides one measure of the quality of the calculation.

In a Hartree–Fock treatment the initial state is represented by a single-configuration state function (CSF) $\chi_0^{\mathrm{i}}(N)$ and the final state by the CSF, $\chi_n^{\mathrm{f}}(N)$, where

$$\chi_n^{\mathrm{f}}(N) = A\{\psi_{\epsilon_n}^{\mathrm{f}}(1)\,\chi_n^{\mathrm{f}}(N-1)\}\,. \tag{3}$$

Here $\chi_n^{\mathrm{f}}(N)$ is the antisymmetrised product of the final ion CSF $\chi_n^{\mathrm{f}}(N-1)$ with the continuum function $\psi_{\epsilon_n}^{\mathrm{f}}$, which is normalised to unit outgoing energy.

(b) Photoionisation angular distribution

Photoionisation by an electric dipole interaction between linearly polarised radiation and randomly oriented target molecules (Yang 1948; Cooper and Zare 1969) gives rise to a differential cross section of the form

$$\mathrm{d}\sigma/\mathrm{d}\Omega = (\sigma_{\mathrm{tot}}/4\pi)\{1+\beta P_2(\cos\theta)\}\,, \tag{4}$$

where σ_{tot} is the angle-integrated total cross section, θ is the ejection angle of the photoelectron relative to the polarisation vector of the incident radiation, and $P_2(\cos\theta) = \frac{1}{2}(3\cos^2\theta - 1)$. The angular distribution is determined completely by the asymmetry parameter β, the value of which is physically confined to the range $-1 \leqslant \beta \leqslant 2$. The analysis by Tully *et al.* (1968) gives the vibrationally and rotationally unresolved differential cross section of a linear molecule as

$$\mathrm{d}\sigma/\mathrm{d}\Omega = \tfrac{4}{3}\pi^2\alpha h\nu \sum_{J=0,2} A_J\,P_J(\cos\theta)\,, \tag{5}$$

$$\begin{aligned} A_J = \sum_{L_1 L_2 \lambda_1 \lambda_2} & (-1)^{\Lambda_{\mathrm{f}}+\Lambda_{\mathrm{i}}}(2J+1)^{-1}\{(2L_1+1)(2L_2+1)\}^{\frac{1}{2}} \\ & \times C(11J\,|\,\Lambda_{\mathrm{i}}-\Lambda_{\mathrm{f}}-\lambda_1,\,\Lambda_{\mathrm{f}}-\Lambda_{\mathrm{i}}+\lambda_2) \\ & \times C(11J\,|\,00)\,C(L_2\,L_1\,J\,|\,\lambda_2,-\lambda_1)\,C(L_2\,L_1\,J\,|\,00) \\ & \times \mathrm{i}^{L_2-L_1}\exp\{\mathrm{i}(\delta_{L_1\lambda_1}-\delta_{L_2\lambda_2})\}\,M_{L_1\lambda_1}\,M^*_{L_2\lambda_2}\,, \end{aligned} \tag{6}$$

and hence

$$\beta = A_2/A_0\,. \tag{7}$$

The quantum numbers L and λ asymptotically characterise the final state continuum angular momentum states; Λ_{i} and Λ_{f} are the magnetic quantum numbers of the initial state and the final ion core state respectively, $C(j_1\,j_2\,J\,|\,m_1\,m_2)$ are Clebsch–Gordan coefficients, and $h\nu$ $(=\epsilon + I_{\mathrm{if}})$ is the incident photon energy. The asymmetry parameter for a given system is then determined by the continuum phase shifts $\delta_{L\lambda}$ and dipole transition moments $M_{L\lambda}$ for each of the allowed final state continuum channels. The phase shifts are fixed by the asymptotic radial form of the continuum wavefunction, which is the Coulomb function (Abramowitz 1972) with argument

$$\Theta_{L\lambda} = kr + (Z_n/k)\ln(2kr) - \tfrac{1}{2}L\pi + \delta_{L\lambda}\,, \tag{8}$$

where k is the photoelectron momentum and Z_n is the net charge on the final state molecular core. The transition moments are given by

$$M_{L\lambda} = \langle \Psi^{\mathrm{f}}_{L\lambda} | \sum_j d_j | \Psi^{\mathrm{i}} \rangle . \tag{9}$$

In the present work expressions for A_0 and A_2 are required for photoionisation from a σ_g or σ_u initial state orbital. Expressions for the σ_g case are given elsewhere (Richards and Larkins 1986). By writing the interaction term as

$$\Delta(L_1 \lambda_1, L_2 \lambda_2) = \exp\{\mathrm{i}(\delta_{L_1\lambda_1} - \delta_{L_2\lambda_2})\} M_{L_1\lambda_1} M^*_{L_2\lambda_2},$$

and including terms up to $L = 5$, the expressions for A_J in the σ_u case with $\Lambda_i = \Lambda_f = 0$ are

$$\begin{aligned} A_0 = {} & \tfrac{1}{3}\Delta(00,00) + \tfrac{1}{3}\Delta(20,20) + \tfrac{2}{3}\Delta(21,21) \\ & + \tfrac{1}{3}\Delta(40,40) + \tfrac{2}{3}\Delta(41,41), \end{aligned} \tag{10}$$

$$\begin{aligned} A_2 = {} & -\tfrac{4}{15}\sqrt{5}\,\Delta(00,20) - \tfrac{4}{15}\sqrt{15}\,\Delta(00,21) + \tfrac{4}{21}\Delta(20,20) + \tfrac{4}{21}\sqrt{3}\,\Delta(20,21) \\ & + \tfrac{10}{21}\Delta(21,21) - \tfrac{8}{35}\sqrt{5}\,\Delta(20,40) - \tfrac{4}{7}\sqrt{2}\,\Delta(20,41) + \tfrac{16}{105}\sqrt{15}\,\Delta(21,40) \\ & + \tfrac{8}{21}\sqrt{6}\,\Delta(21,41) + \tfrac{1}{1284}\sqrt{49434}\,\Delta(40,40) + \tfrac{4}{77}\sqrt{10}\,\Delta(40,41) \\ & + \tfrac{16}{1847}\sqrt{1847}\,\Delta(41,41). \end{aligned} \tag{11}$$

(c) Li_2 continuum wavefunction evaluation

The details of the two-dimensional numerical treatment of molecular continuum wavefunctions have been outlined previously (Richards and Larkins 1984, 1986). At the Hartree–Fock level the equation to describe a continuum electron of energy ϵ in the field of a bound-state molecular core comprising $(N-1)$ electrons, abbreviated ψ_ϵ, is

$$\left(H_\epsilon + \sum_j \alpha_j J_j - \sum_j{}' \beta_j K_j - \epsilon \right) \psi_\epsilon(1) = 0, \tag{12}$$

where

$$H_\epsilon = -\tfrac{1}{2}\nabla^2(1) - \sum_\mu \frac{Z_\mu}{r_{\mu\epsilon}}, \tag{13}$$

$$J_j \psi_\epsilon(1) = \left(\int \frac{\psi_j^2(2)}{r_{12}} \, \mathrm{d}\tau_2 \right) \psi_\epsilon(1), \tag{14}$$

$$K_j \psi_\epsilon(1) = \left(\int \frac{\psi_j(2)\psi_\epsilon(2)}{r_{12}} \, \mathrm{d}\tau_2 \right) \psi_j(1). \tag{15}$$

Here the subscript μ refers to atomic nuclei (of charge $+Z_\mu$) in the molecule, and the subscript j refers to the bound-state orbitals; $\Sigma_j \alpha_j J_j$ represents the molecular

Coulomb potential and $\Sigma_j' \beta_j K_j$ represents the molecular exchange potential, and the coefficients α_j and β_j are characterised by the symmetry of the total N-electron state (Roothaan 1960).

The numerical treatment consists of performing a conventional algebraic basis set calculation on the initial and final ionic core bound states and then solving for the photoelectron continuum wavefunction numerically, in the relaxed Hartree–Fock ion core potential derived from the bound state calculation.

In the present work an (11s, 6p) uncontracted gaussian set from Huzinaga and coworkers was used for the Hartree–Fock initial and final ion core bound state calculations (11s from Huzinaga *et al.* 1971; 6p from Huzinaga 1965). The cross section and angular distribution results reported here correspond to the use of the relaxed Hartree–Fock model.

(d) Auger transition rates

The Auger process involves a radiationless transition between a highly excited initial $(N-1)$-electron state ψ^{i}_m, and a final state ψ^{f}_n consisting of an $(N-2)$-electron bound state and a free Auger electron of energy ϵ,

$$\epsilon = E^{\mathrm{f}}_n - E^{\mathrm{i}}_m . \tag{16}$$

The many-electron Hamiltonian of a system undergoing a radiationless transition is given by

$$H = H_0 + H_{\mathrm{C}} + H_{\mathrm{so}} , \tag{17}$$

where

$$H_{\mathrm{C}} = \sum_{i>j} 1/r_{ij}$$

is the Coulomb interaction between electron pairs,

$$H_0 = \sum_i (-\tfrac{1}{2}\nabla_i^2) - \sum_{\mu,i} Z_\mu / r_{\mu i}$$

is the remainder of the nonrelativistic Hamiltonian, and H_{so} is the relativistic spin–orbit interaction. The transition probability for an Auger transition from ψ^{i}_m to ψ^{f}_n is given from first order perturbation theory (Wentzel 1927) by

$$P_{\mathrm{if}} = 2\pi \rho(E^{\mathrm{f}}_n) |\langle \psi^{\mathrm{f}}_n | H_0 - E^{\mathrm{i}}_m | \psi^{\mathrm{i}}_m \rangle|^2 , \tag{18}$$

where $\rho(E^{\mathrm{f}}_n)$ is the energy density of states about the final state energy.

The Auger transition can be treated in various coupling schemes, either Russell–Saunders, *jj*, or intermediate coupling (Asaad and Burhop 1958). For the molecules of interest in the present work consisting of low Z nuclei, Russell–Saunders coupling applies, that is Λ and S are conserved in the transition for linear molecules, and a nonrelativistic treatment is appropriate. In the nonrelativistic limit the perturbation in the transition operator (18) reduces to the Coulomb interaction between the electrons participating in the transition. In the Hartree–Fock approximation, single

configuration state functions are used to represent ψ^i_m and ψ^f_n:

$$\psi^i_m = \chi^i_m(N-1), \tag{19}$$

$$\psi^f_n = A\{\psi^f_{\epsilon_n}(1)\chi^f_n(N-2)\}. \tag{20}$$

If different orbital sets are used to construct the bound states χ^i_m and χ^f_n the transition probability expression (18) becomes complex to evaluate, although the appropriate formalism exists (Howat *et al.* 1978). If, however, a frozen core approximation is made, in which the final state is constructed from the initial state orbital set, the transition probability reduces to an expression in terms of the Coulomb and exchange integrals (Siegbahn *et al.* 1975)

$$J_{ab} = \langle\psi^i_a\psi^i_b|1/r_{12}|\psi^f_c\psi^f_\epsilon\rangle, \qquad K_{ab} = \langle\psi^i_b\psi^i_a|1/r_{12}|\psi^f_c\psi^f_\epsilon\rangle, \tag{21}$$

involving the continuum orbital $\psi^f_{\epsilon_n}$, the final state orbital ψ^f_c in which a vacancy is present in the initial state ion, and the initial state orbitals ψ^i_a and ψ^i_b which correspond to the vacancies produced in the final state by the ejection of the Auger electron and the filling of the existing initial state vacancy. Expressions for the transition probability are given by Ågren (1981) for both initially closed and open shell molecules.

3. Results

(a) Li_2 cross sections

Photoionisation cross sections and angular distributions were calculated for the core ionisation processes

$$\mathrm{Li_2}\,[\text{—}]({}^1\Sigma_g^+) \xrightarrow{h\nu} \mathrm{Li_2^+}\,[1\sigma_g]({}^2\Sigma_g^+) \begin{cases} \epsilon\pi_u({}^1\Pi_u) \\ \epsilon\sigma_u({}^1\Sigma_u^+) \end{cases}, \tag{22}$$

$$\mathrm{Li_2}\,[\text{—}]({}^1\Sigma_g^+) \xrightarrow{h\nu} \mathrm{Li_2^+}\,[1\sigma_u]({}^2\Sigma_u^+) \begin{cases} \epsilon\pi_g({}^1\Pi_u) \\ \epsilon\sigma_g({}^1\Sigma_u^+) \end{cases}, \tag{23}$$

and for the valence ionisation process

$$\mathrm{Li_2}\,[\text{—}]({}^1\Sigma_g^+) \xrightarrow{h\nu} \mathrm{Li_2^+}\,[2\sigma_g]({}^2\Sigma_g^+) \begin{cases} \epsilon\pi_u({}^1\Pi_u) \\ \epsilon\sigma_u({}^1\Sigma_u^+) \end{cases}. \tag{24}$$

The ground state equilibrium geometry of $R = 5{\cdot}052$ a.u. (Huber and Herzberg 1979) was used in all calculations. The bound state SCF wavefunctions were evaluated using an uncontracted (11s, 6p) gaussian basis set, as mentioned previously. The final core state was described in a relaxed orbital approach. Calculations were performed using the UIBMOL SCF program package (Faegri and Manne 1976). The total SCF energies for the molecular states are given in Table 1. While lower total energies result from multiconfiguration calculations which include correlation (Schwarz *et al.* 1978; Bacskay *et al.* 1986) the SCF approach was considered adequate to generate the $N-1$ electron potential required for the determination of molecular continuum functions.

The calculated ΔSCF ionisation energies for photoemission from $1\sigma_g$, $1\sigma_u$ and $2\sigma_g$ orbitals are 64·68, 64·63 and 4·38 eV respectively. These theoretical values have been used for specifying ionisation thresholds required for the transition moment calculations. The only ionisation energy known experimentally with reasonable confidence is the $2\sigma_g$ adiabatic ionisation potential of 5·14 eV (Eisel *et al.* 1983; Bernheim *et al.* 1983) which is not directly comparable with the Franck–Condon value.

Table 1. Total Hartree–Fock SCF energies for the molecular states of the Li_2 molecule

Electronic configuration[A]	Energy[B] (a.u.)
Li_2 [—] $^1\Sigma_g^+$	−14·8713
Li_2^+ [$1\sigma_g$] $^2\Sigma_g^+$	−12·4944
[$1\sigma_u$] $^2\Sigma_u^+$	−12·4962
[$2\sigma_g$] $^2\Sigma_g^+$	−14·7103
Li_2^{2+} [$2\sigma_g^2$] $^1\Sigma_g^+$	−14·2750

[A] Hole state notation has been used. The change in the electronic configuration from the ground state configuration $1\sigma_g^2 1\sigma_u^2 2\sigma_g^2$ is indicated in square brackets.
[B] SCF energies evaluated at R_e = 5·052 a.u. with a (11s, 6p) gaussian basis set.

The photoionisation properties for continuum angular momentum states to $L = 5$ for u symmetry and to $L = 4$ for g symmetry at photoelectron energies up to 6·0 a.u. have been determined. As in previous work L coupling between the exit channels has been neglected. The Li_2 ground state equilibrium bond length of over 5 a.u. is one of the largest of the first row diatomics. It is significantly longer than for the diatomic molecules H_2 (R_e = 1·4 a.u.) and H_2^+ (R_e = 2·0 a.u.) which we have considered previously using the numerical method. From the physical point of view it is of interest to assess the extent to which the ionisation process retains atomic-like character at this large internuclear separation. From the numerical point of view, however, the large bond length is troublesome. It means that a finer grid spacing is needed and, since the molecular potential approaches its asymptotic form more slowly, the grid must extend further. Moreover, the larger bond length causes the influence of L coupling in the continuum wavefunction to be larger. The overall result is that for numerical calculations of a given size, lower numerical accuracy is obtained for Li_2 cross sections than for H_2 or H_2^+. Various numerical (r, θ) grid arrangements were used, with grid spacings h = 0·051–0·084 a.u. and $\delta\theta = \frac{1}{60}\pi - \frac{1}{40}\pi$, and boundary values r_B = 25–38 a.u. The Li_2 exchange potential calculation converged more slowly than the H_2 calculation, and 5–15 iterations were generally necessary compared with 3–10 for the H_2 molecule. The numerical normalisation angular consistency was of the order of $\Delta A/A$ = 1% at ϵ = 0 a.u. increasing to 10%–30% at ϵ = 2·0 a.u. and 30%–50% at ϵ = 6·0 a.u. The angular consistency in the numerical phase shift varied between $\pm 0{\cdot}005\pi$ at threshold and $\pm 0{\cdot}04\pi$ at ϵ = 6·0 a.u. Cross sections are generally numerically converged to 0·02 Mb and phase shifts to $0{\cdot}01\pi$. Because of the large bond length and the neglect of L coupling, uncertainties in the absolute values are estimated to be from 10% to 30%.

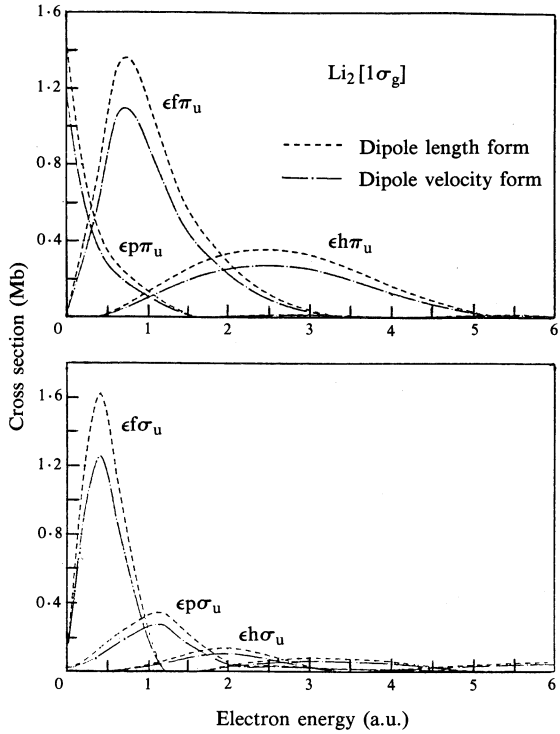

Fig. 1. Partial channel cross sections for $Li_2[1\sigma_g]$ photoionisation, $L = 1, 3, 5$.

Fig. 1&2.

Fig. 2. Partial channel cross sections for $Li_2[1\sigma_u]$ photoionisation, $L = 0, 2, 4$.

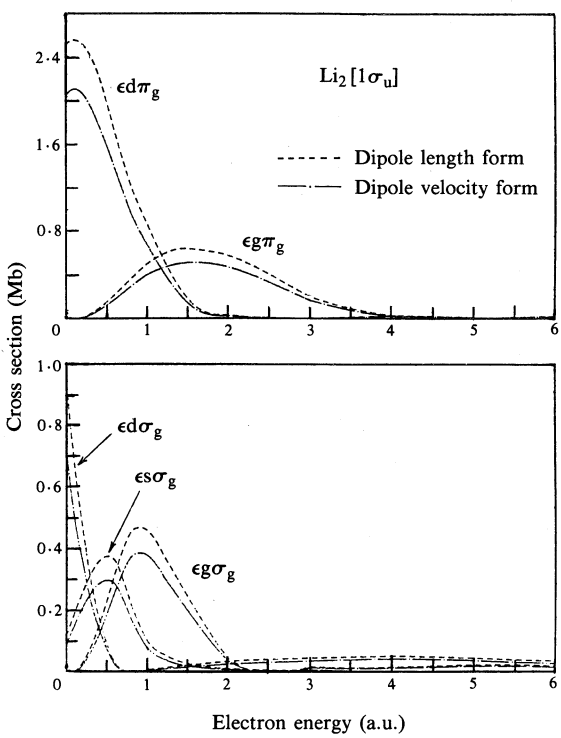

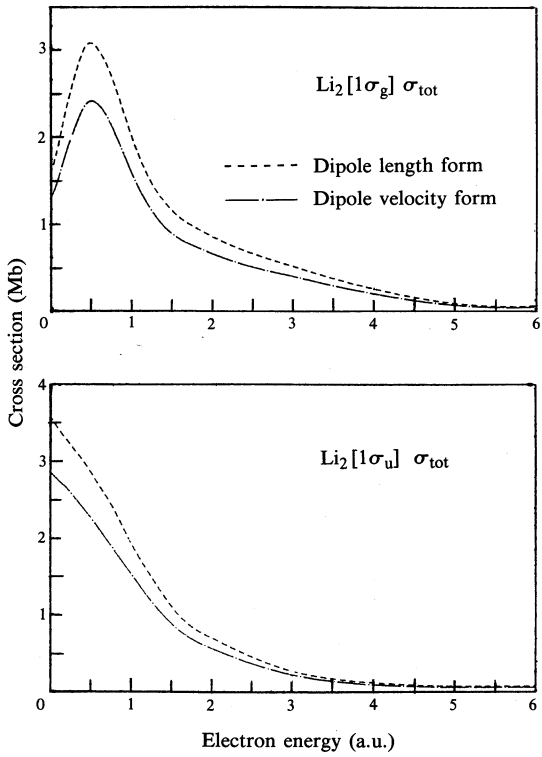

Fig. 3. Partial cross section for $Li_2[1\sigma_g]$ and $Li_2[1\sigma_u]$ photoionisation.

Table 2. Lithium molecule photoionisation cross sections for core and valence shell ionisation

Electron energy (a.u.)	Cross section[A] (Mb)			
	$1\sigma_g + 1\sigma_u$		$2\sigma_g$	
	L	V	L	V
0·00	5·175	4·163	1·260	0·086
0·05	5·240	4·209	1·610	1·402
0·10	5·353	4·296	1·929	1·783
0·20	5·648	4·517	2·294	2·135
0·30	5·858	4·641	2·272	2·077
0·40	6·008	4·734	2·002	1·770
0·60	5·631	4·490	1·317	1·044
0·80	4·823	3·830	0·854	0·557
1·00	3·931	3·118	0·559	0·362
1·20	3·128	2·467	0·382	0·277
1·40	2·516	1·967	0·245	0·203
1·60	2·052	1·615	0·181	0·142
1·80	1·763	1·389	0·135	0·102
2·00	1·548	1·216	0·117	0·081
3·00	0·778	0·615	0·050	0·033
4·00	0·369	0·287	0·021	0·015
5·00	0·158	0·125	0·007	0·004
6·00	0·137	0·107	0·002	0·002

[A] Absolute uncertainties are estimated to be from 10% to 30% due to the long bond length and the neglect of L coupling. More significant figures are listed to provide an insight into the agreement between the length (L) and velocity (V) forms.

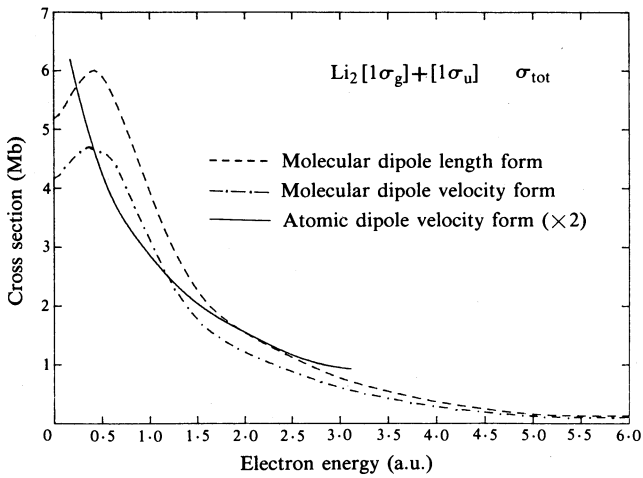

Fig. 4. Sum of the Li_2 cross section for $1\sigma_g$ and $1\sigma_u$ core photoionisation. The atomic Li 1s cross section multiplied by 2 is also shown.

(i) *Core Ionisation Cross Sections*

The partial channel cross sections for $1\sigma_g$ ionisation into π_u and σ_u continuum channels corresponding to angular momentum states $L = 1, 3, 5$ up to an electron energy of 6·0 a.u. are presented in Fig. 1. The partial channel cross sections for $1\sigma_u$ ionisation into π_g and σ_g continuum channels corresponding to angular momentum states $L = 0, 2, 4$ are presented in Fig. 2. Values for both the dipole length and dipole velocity forms are presented. The resultant partial photoionisation cross sections for the $1\sigma_g$ and $1\sigma_u$ orbitals are shown in Fig. 3. Since the binding energy difference between the $1\sigma_g$ and $1\sigma_u$ orbitals is very small —the present SCF calculations indicate ~0·05 eV, while multiconfiguration Hartree–Fock (MCHF) calculations indicate an even smaller splitting—, it is unlikely that the experimentalist will resolve the peaks for the two processes. The sum of the $1\sigma_g$ and $1\sigma_u$ partial cross sections is given in Table 2 and Fig. 4. The corresponding core photoionisation cross section for atomic lithium using standard atomic numerical Hartree–Fock procedures (Larkins *et al.* 1981, unpublished) and the dipole velocity form of the operator is also included in Fig. 4 for comparison with the molecular cross section. The same level of approximation was applied in the atomic calculation as in the molecular calculation, namely a Hartree–Fock approach with exchange and a relaxed final state potential. There are some difficulties with the atomic calculations due to the complex final state shake-up and conjugate shake-up processes since one must consider the processes

$$\text{Li } 1s^2 2s(^2S) \xrightarrow{h\nu} \text{Li}^+ \; 1s2s(^{1,3}S)\,\epsilon p(^2P^0), \tag{25}$$

$$\text{Li } 1s^2 2s(^2S) \xrightarrow{h\nu} \text{Li}^+ \; 1s2p(^{1,3}P^0)\,\epsilon s(^2P^0). \tag{26}$$

Nevertheless, from a comparison with recent preliminary experimental data, the results are considered to be a useful guide to the magnitude of the atomic core hole photoionisation cross sections. The atomic cross section calculations will be discussed in detail in a future publication (Larkins *et al.* unpublished).

The $1\sigma_g$ cross section presented in Fig. 1 is almost entirely $\epsilon p\pi_u$ at threshold, but the $L = 3$ channels become the main components from $\epsilon = 0{\cdot}5$–2 a.u.; at higher energies the $L = 5$ channels also become significant. For $1\sigma_u$ ionisation processes shown in Fig. 2 it is the $L = 2$ channels up to 1 a.u., then $\epsilon s\sigma_g$ and the $L = 4$ channels which dominate. The assertion of Davenport *et al.* (1983) that the $1\sigma_u$ cross section is mainly $L = 1$ must be in error, since only even L components are allowed in $\epsilon\sigma_g$ and $\epsilon\pi_g$ channels. Furthermore, the present work also does not agree with the finding from the multiple scattering calculations of Davenport *et al.* (1983) that the $1\sigma_g$ ionisation is almost wholly in the $L = 3$ channels nor is the double peak

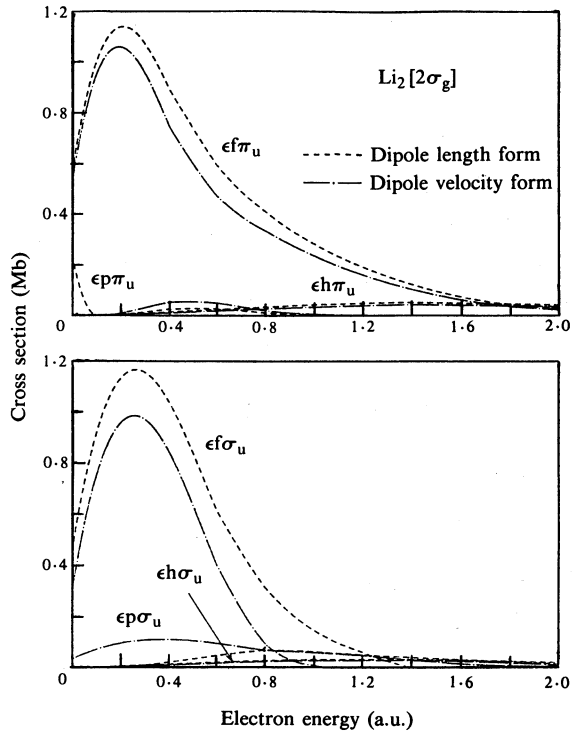

Fig. 5. Partial channel cross sections for $Li_2[2\sigma_g]$ valence photoionisation, $L = 1, 3, 5$.

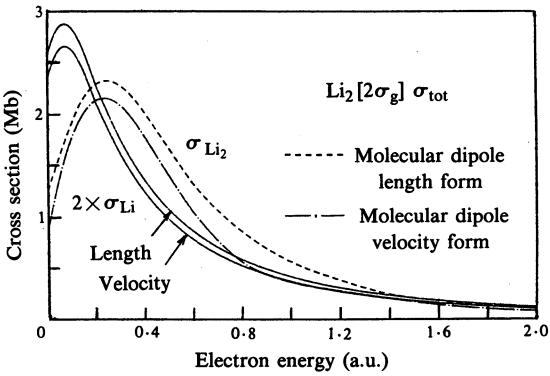

Fig. 6. Total Li_2 cross section for $2\sigma_g$ valence photoionisation. The atomic Li 2s cross section multiplied by 2 is also shown.

structure near threshold (Fig. 4) as strongly pronounced. The multiple scattering calculations also predict cross sections which are more than 50% higher than the present work.

The $1\sigma_g$ and $1\sigma_u$ partial cross sections are very similar at electron energies greater than 0·5 a.u. above threshold; however, at smaller electron energies the $1\sigma_g$ cross section decreases while the $1\sigma_u$ cross section increases. Davenport *et al.* (1983) have reported a similar qualitative behaviour for the two partial cross sections although the absolute magnitudes are higher. Near threshold the different symmetry characteristics of the $1\sigma_g$ orbital, which is s-like in an atomic sense, and the $1\sigma_u$ antibonding orbital, which is p-like, manifest themselves most strongly.

Comparison with the atomic 1s cross section in Fig. 4 shows that the total molecular cross section is near to twice the atomic value, especially at electron energies between 0·5 and 1·5 a.u.

(ii) *Valence Ionisation Cross Sections*

The partial channel cross sections for $2\sigma_g$ ionisation into π_u and σ_u continuum channels corresponding to angular momentum states $L = 1, 3, 5$ are presented in Fig. 5 for both the length and the velocity dipole forms. The total $2\sigma_g$ cross section is presented in Table 2 and Fig. 6. Values are given in Fig. 6 only up to 2·0 a.u. since the cross section falls off more rapidly above this energy than for the core processes. Fig. 6 also includes the atomic lithium 2s cross section calculated at the same level of approximation as for the molecular process. In a Hartree–Fock description, the atomic transition involved is

$$\text{Li } 1s^2 2s(^2S) \xrightarrow{h\nu} \text{Li}^+ \, 1s^2(^1S)\, \epsilon p(^2P^0)\,. \tag{27}$$

The calculated atomic 2s photoionisation cross sections are in good agreement with recent experimental work of Gerard (1984). The $2\sigma_g$ cross section is dominated by the $L = 3$ channels up to 1·5 a.u., above which the $L = 5$ and $L = 1$ channels also become significant (Fig. 5). This result contradicts the multiple scattering result of Davenport *et al.* (1983), in the energy range below 0·5 a.u. that the $L = 1$ contribution dominates the $\epsilon\pi_u$ cross section. The discrepancy can be attributed to the effect of the Hartree–Fock potential compared with the multiple scattering potential, since the effects of L coupling will be small in this energy range. Overall the Hartree–Fock total cross sections are of a similar magnitude to the multiple scattering results, however, the profiles are considerably different in detail when considered as a function of photon energy. In the present work the π_u and σ_u channels show a similar dependence on photon energy. This is not the case with the earlier study.

The molecular valence shell $2\sigma_g$ photoionisation cross section is quantitatively close to twice the atomic Li cross section at photoelectron energies from 1·5 to 6·0 a.u., and is still qualitatively similar at lower energies (Fig. 6). The main deviations occur within 0·2 a.u. of threshold where the molecular cross section is significantly less than twice the atomic cross section. This indicates that the Li_2 photoionisation process is predominantly atomic-like at moderately high energies even in the valence shell, where molecular interference effects can be expected to be larger than in the core shell. This effect has been interpreted (Cooper 1974) for H_2 in terms of the photoionisation matrix element, in which the factor $\exp(i\,\boldsymbol{k}.\boldsymbol{r})$ emphasises the contributions to the matrix element from the region $r < 1/k$ around each nucleus. Since the Li_2 bond length is large, the molecular interference contributions to the matrix element become small at relatively low energies.

The fact that the Li_2 cross section so closely resembles the sum of two atomic cross sections is remarkable since the composition of the atomic matrix element is much simpler, a single s $\rightarrow$ p component in the 2s case, compared with a sum of many different channels, whose relative contributions vary with energy, in the molecular case.

The effect of continuum exchange on the Li_2 core cross sections was found to be similar to the H_2 case reported earlier. The magnitude of the change in individual channel cross sections when exchange was included decreased with increasing energy from a maximum of 15%–25% in the range $\epsilon = 1$ a.u. The largest changes occurred in the low L channels. Above $\epsilon = 2$ a.u., the cross section changes were generally less than 1%–2%. Another notable feature of the core cross sections is that the ratio of the length and velocity cross sections varies little from the value $M_V/M_L = 0{\cdot}89$ ($\sigma_V/\sigma_L = 0{\cdot}79$) across the whole energy range. The consistency of the length and velocity forms is not as predictable in the valence cross section, although the shapes of the length and velocity cross section curves are generally similar.

(b) Angular distributions

Continuum phase shifts ($\delta_{L\lambda} - \sigma_L$) are presented for $1\sigma_g$, $1\sigma_u$ and $2\sigma_g$ ionised Li_2^+ continuum wavefunctions up to $L = 5$ in Fig. 7. The corresponding asymmetry parameters are presented in Fig. 8 and Table 3 for $1\sigma_g$, $1\sigma_u$ and $2\sigma_g$ ionisation, as well as the combined asymmetry parameter for the core processes, given by

$$\beta_{1\sigma_g+1\sigma_u} = (\beta_{1\sigma_g}\sigma_{1\sigma_g} + \beta_{1\sigma_u}\sigma_{1\sigma_u})/(\sigma_{1\sigma_g} + \sigma_{1\sigma_u}). \tag{28}$$

The asymmetry parameters are presented up to $\epsilon = 2{\cdot}0$ a.u., since at higher energies the reliability of the phase shifts is reduced due to the increased importance of L coupling, and the cross sections are sufficiently small that the numerical accuracy becomes significant in the asymmetry parameter. There is considerably more structure in the Li_2 1σ β values compared with the H_2 case reported earlier (Richards and Larkins 1986). The H_2 β value is relatively constant with energy since the cross section is dominated by certain angular momentum components. The Li_2 β values pass through a series of maxima and minima corresponding to the changing composition of the total cross section. For example, the β minimum for $1\sigma_g$ at $\epsilon \sim 1{\cdot}0$ a.u. is caused by the maximum in the $\epsilon f\pi_u$ cross section coupled with the rapidly decreasing $\epsilon f\sigma_u$ cross section. Similarly the sharp increase in β for $1\sigma_u$ at threshold corresponds to a decrease in the $L = 2$ cross sections. There is close agreement between core β values calculated with the length and the velocity forms of the transition moments. The valence $2\sigma_g$ β values show a significantly different dependence on electron energy to the 1σ β values. The variation between the length and velocity forms is also larger. Experimental Li_2 β values should provide a sensitive test of various theoretical models.

(c) Li_2 Auger transition rates

Auger transitions are energetically possible from each of the core ionised Li_2^+ states to a single Li_2^{2+} final state,

$$Li_2^+ [1\sigma_g](^2\Sigma_g^+) \rightarrow Li_2^{2+} [2\sigma_g^2](^1\Sigma_g^+)\epsilon\sigma_g(^2\Sigma_g^+), \tag{29}$$

$$Li_2^+ [1\sigma_u](^2\Sigma_u^+) \rightarrow Li_2^{2+} [2\sigma_g^2](^1\Sigma_g^+)\epsilon\sigma_u(^2\Sigma_u^+). \tag{30}$$

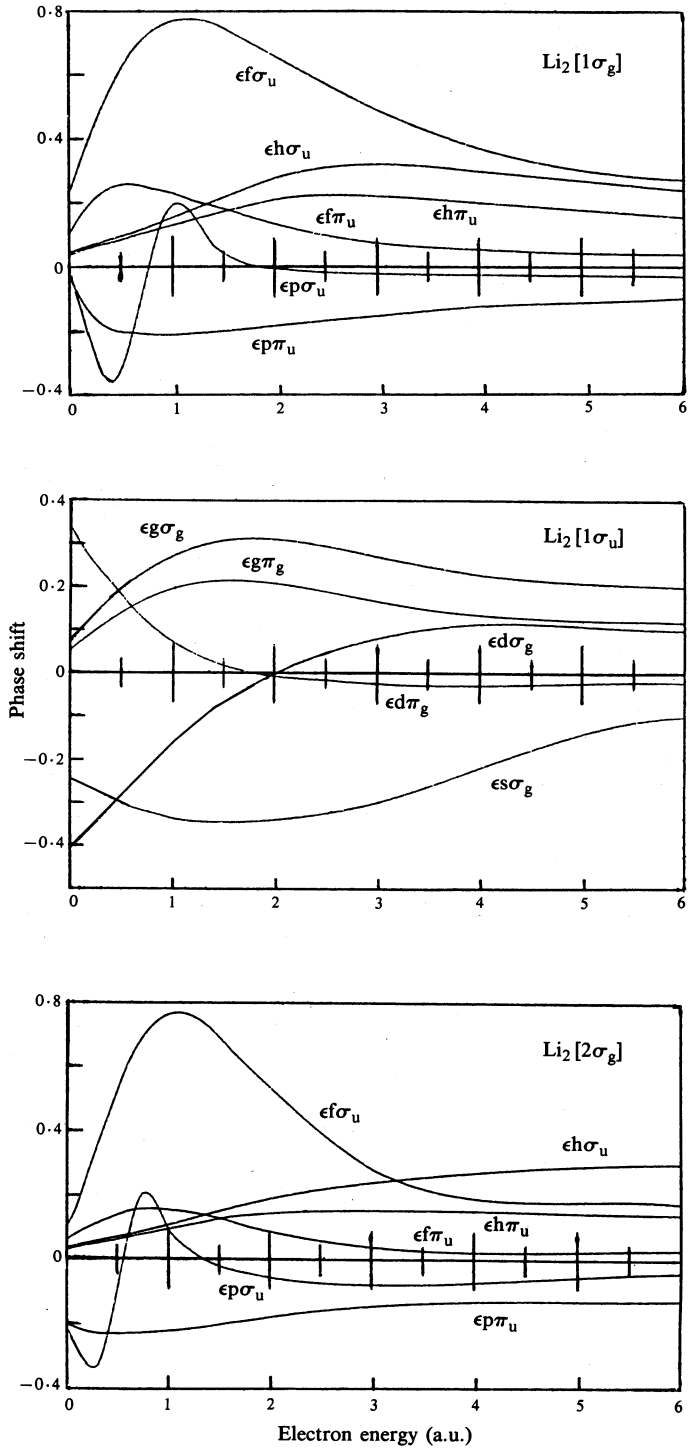

Fig. 7. Continuum phase shifts $(\delta_{L\lambda} - \sigma_L)/\pi$ for continuum wavefunctions associated with ionised Li_2^+ $[1\sigma_g]$, Li_2^+ $[1\sigma_u]$ and Li_2^+ $[2\sigma_g]$.

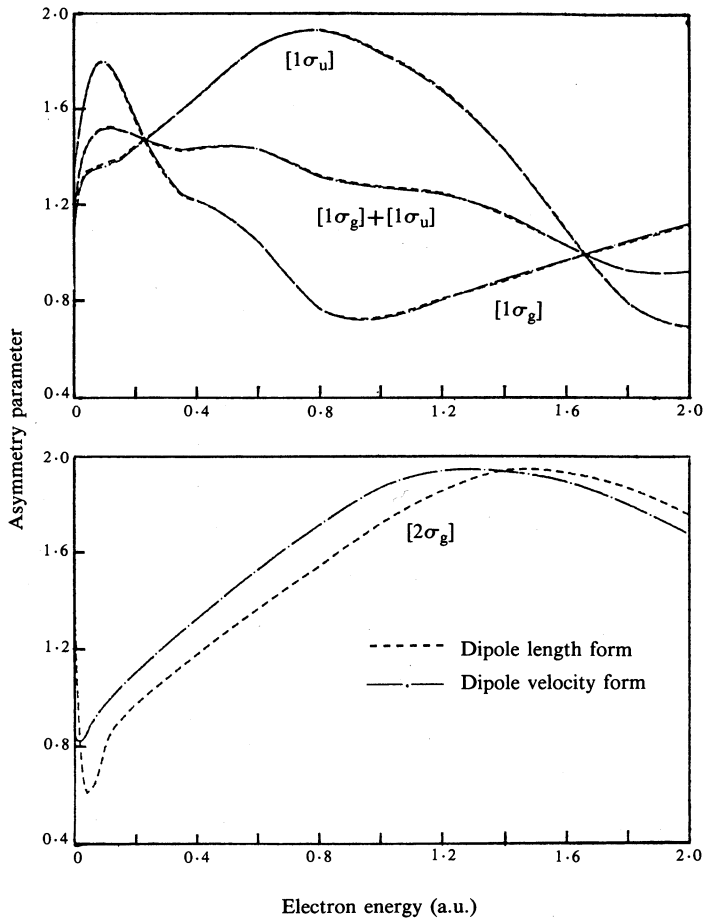

Fig. 8. Asymmetry parameters β for Li_2 photoionisation, $1\sigma_g$, $1\sigma_u$ and $2\sigma_g$ orbitals and combined core ionisation $1\sigma_g + 1\sigma_u$ (see equation 28).

Table 3. Lithium molecule asymmetry parameters for core and valence shell ionisation[A]

Electron energy (a.u.)	$\beta_{1\sigma_u}$ L	V	$\beta_{1\sigma_g}$ L	V	$\beta_{1\sigma_g+1\sigma_u}$[B] L	V	$\beta_{2\sigma_g}$ L	V
0·00	1·093	1·083	1·337	1·320	1·168	1·157	1·336	0·843
0·050	1·346	1·336	1·719	1·721	1·469	1·464	0·623	0·888
0·100	1·374	1·362	1·794	1·799	1·525	1·518	0·808	0·936
0·200	1·449	1·442	1·546	1·559	1·490	1·490	0·956	1·337
0·300	1·545	1·544	1·316	1·325	1·439	1·441	1·035	1·296
0·400	1·649	1·652	1·217	1·220	1·434	1·439	1·104	1·320
0·600	1·863	1·863	1·048	1·049	1·431	1·435	1·317	1·514
0·800	1·932	1·930	0·769	0·768	1·312	1·314	1·535	1·717
1·000	1·841	1·835	0·737	0·730	1·279	1·274	1·701	1·873
1·200	1·684	1·677	0·848	0·842	1·270	1·263	1·859	1·942
1·400	1·432	1·429	0·927	0·936	1·180	1·186	1·943	1·938
1·600	1·097	1·091	0·970	0·971	1·029	1·030	1·932	1·895
1·800	0·794	0·791	1·042	1·049	0·928	0·927	1·869	1·800
2·000	0·691	0·696	1·117	1·124	0·924	0·925	1·757	1·677

[A] See footnote Table 2.
[B] See equation (28).

As in the cross section case, the total transition probability is composed of a sum over all possible angular momentum channels in $\epsilon\sigma_g$ and $\epsilon\sigma_u$. Values of $L = 0, 2, 4$ are included for the σ_g channel and values of $L = 1, 3, 5$ for the σ_u channel. The continuum wavefunctions were evaluated at the ΔSCF Auger energies which for the two processes given in equations (29) and (30), using the data in Table 1, are 48·45 and 48·40 eV respectively. The Li_2 Auger energies are not known experimentally, but the calculated values may be compared with the MCSCF estimate by Bacskay *et al.* (1986) of 45·3 eV. Numerical grid parameters of $h = 0{\cdot}032$–$0{\cdot}051$ a.u., $\delta\theta = \frac{1}{80}\pi - \frac{1}{40}\pi$, and $r_B = 15{\cdot}2$–$25{\cdot}3$ a.u. were employed to evaluate the continuum wavefunctions.

In the present work the Auger transition rates were calculated with the final state potential generated in a frozen orbital approach, in which the Li_2^{2+} bound wavefunction was constructed from the appropriate initial state Li_2^+ functions. The exchange potential between the continuum electron and the frozen core was included. In this description, the transition probability for the two Auger processes can be expressed in the form

$$P_{if} = 2\pi |J_c|^2, \tag{31}$$

where, for transition (29),

$$J_{1\sigma_g} = \langle 2\sigma_g^i 2\sigma_g^i | 1/r_{12} | 1\sigma_g^f \epsilon\sigma_g^f \rangle \tag{32}$$

and, for transition (30),

$$J_{1\sigma_u} = \langle 2\sigma_g^i 2\sigma_g^i | 1/r_{12} | 1\sigma_u^f \epsilon\sigma_u^f \rangle. \tag{33}$$

Table 4. Auger emission transition probabilities from core ionised Li_2^+ initial states

Frozen core Hartree–Fock calculation with exchange

Continuum channel	Transition prob. (10^{-4} a.u.)	Continuum channel	Transition prob. (10^{-4} a.u.)
$Li_2^+ [1\sigma_g] \rightarrow Li_2^{2+} [2\sigma_g^2] + \epsilon L\sigma_g$		$Li_2^+ [1\sigma_u] \rightarrow Li_2^{2+} [2\sigma_g^2] + \epsilon L\sigma_u$	
$\epsilon s\sigma_g$	2·3	$\epsilon p\sigma_u$	1·6
$\epsilon d\sigma_g$	0·3	$\epsilon f\sigma_u$	0·3
$\epsilon g\sigma_g$	0·0	$\epsilon h\sigma_u$	0·0
$\epsilon\sigma_g$ total	2·6	$\epsilon\sigma_u$ total	1·9

The calculated Li_2 Auger transition probabilities are presented in Table 4. The numerical accuracy of the values is 5–10%, the largest values being the most accurate. The Auger matrix element is more sensitive to numerical evaluation than the photoionisation matrix element, because of the smaller magnitude of the integral ($\sim 10^{-3}$ a.u.) which results from cancellation between large positive and negative components produced by the oscillating continuum wavefunction.

The transition probabilities for the Li_2 $1\sigma_g$ and $1\sigma_u$ Auger processes are predicted by the frozen core Hartree–Fock model to be similar in magnitude, $2{\cdot}6\times10^{-4}$ and $1{\cdot}9\times10^{-4}$ a.u. respectively. Because of the closeness of the transition energies of the two processes (<0·05 eV), independent experimental Li_2 Auger data for both transitions will be very difficult to acquire. The relative intensity of the two transitions depends both on the Auger decay rates and, since different initial Li_2^+ states are involved, on the cross sections for the primary ionisation to produce Li_2^+. The data in Fig. 3 show that near threshold the two initial hole state populations may be

very different. If experimental energies and intensities can be resolved, they will be informative in both the Auger and photoionisation problems.

4. Comparison with Experimental Data

The Li_2 cross section information can be used to clarify some anomalies in the core photoelectron spectrum of lithium metal vapour reported by Krummacher *et al.* (1982). In the published spectrum a set of electron emission peaks was reported at electron energies in the vicinity of 52 eV. A re-analysis of the kinetic energy scale in the published spectrum located the peaks at 51·6 and 52·8 eV (P. Gerard and F. Wuilleumier 1985; unpublished). The two peaks have been assigned as molecular Auger lines, because their electron kinetic energies are independent of photon energy. The observed lines have been shown to display a complex relationship between their intensity and such factors as incident photon energy and furnace temperature.

The observed lines are not molecular diagram Auger lines resulting from transitions (29) and (30) as postulated because their kinetic energies ($\sim$52 eV) and splitting ($\sim$1·2 eV) are too high compared with the best available calculation. They are also not atomic autoionising lines because the excitation energies for the most probable states as given by Ziem *et al.* (1975) are not in agreement with experimental observation. The position of the lines is consistent with them being assigned to molecular autoionising lines associated with the neutral excited species, $Li_2^*(1\sigma^3 2\sigma_g^2 n\phi^1)$. Autoionising lines corresponding to $n\phi^1$ being $1\pi_u$, $2\sigma_u$, $3\sigma_g$ and $1\pi_g$ have been observed at energies of 51·5, 51·6, 52·8 and 53·9 eV respectively (Schwarz *et al.* 1978). The more difficult task is to explain the experimental observation that these molecular lines have an intensity of $\sim$30% of the atomic photoelectron lines in the range 64–68 eV, when under the experimental conditions using a furnace temperature between 400 and 500°C the lithium vapour contains less than 1% dimers (Douglas *et al.* 1955; Stull and Prophet 1977). At 1% relative abundance of Li_2 molecules, a molecular photoexcitation cross section at least one order of magnitude larger than the atomic photoionisation cross section is required to explain the observation. No such enhancement was found in the present work, for the photoionisation process. Assuming that there is not a large deviation from the thermodynamic dimer population in the experiments under discussion and that the effect is due to gas phase processes, it is concluded that the intensity enhancement of the molecular autoionisation lines must result as a consequence of ion–molecule collision phenomena rather than photoexcitation phenomena. A possible mechanism to account for the observations is as follows:

(i) atomic excitation and photoionisation:

$$\mathrm{Li}(1s^2 2s) + h\nu \rightarrow \mathrm{Li}^*(1s\, nl\, nl'), \tag{34}$$

$$\rightarrow \mathrm{Li}^+(1s\, nl) + e; \tag{35}$$

(ii) atom– or ion–molecule collisions:

$$\mathrm{Li}^*(1s\, nl\, nl') + \mathrm{Li}_2(1\sigma^4 2\sigma_g^2) \rightarrow \mathrm{Li}(1s^2 2s) + \mathrm{Li}_2^*(1\sigma^3 2\sigma_g^2 n\phi^1), \tag{36}$$

$$\mathrm{Li}^+(1s\, nl) + \mathrm{Li}_2(1\sigma^4 2\sigma_g^2) \rightarrow \mathrm{Li}^+(1s^2) + \mathrm{Li}_2^*(1\sigma^3 2\sigma_g^2 n\phi^1); \tag{37}$$

(iii) molecular autoionisation:

$$\mathrm{Li}_2^*(1\sigma^3 2\sigma_g^2 n\phi^1) \rightarrow \mathrm{Li}_2^+(1\sigma^4 2\sigma_g) + e'. \tag{38}$$

This mechanism provides for no enhanced molecular contribution to the photoelectron lines in the region 64–68 eV beyond direct molecular photoionisation which will contribute less than 2% to the total intensity. A recognition of this fact requires a re-analysis of the photoelectron lines in the work of Krummacher *et al.* (1982) to determine atomic cross sections. Steps (36) or (37) are required to have high cross sections. It is well established that ion–atom cross sections for inner shell excitation and ionisation can be several orders of magnitude greater than photon or electron impact cross sections (Fano and Lichten 1965; Larkins 1972). A similar mechanism for excitation may be applicable here. A more definite experimental study is required.

Acknowledgments

One of us (J.A.R.) thanks the Aileen S. Andrew Foundation for generous financial support. The continued support of the Australian Research Grants Scheme is also gratefully acknowledged. We also thank P. Gerard and F. Wuilleumier for access to experimental data prior to publication.

References

Abramowitz, M. (1972). *In* 'Handbook of Mathematical Functions' (Eds M. Abramowitz and I. A. Stegun), Applied Mathematics Series 55 (National Bureau of Standards: Washington, D.C.).

Ågren, H. (1981). *J. Chem. Phys.* **75**, 1267.

Amusia, M. Ya., Cherepkov, N. A., Zivanovic, Dj., and Radojevic, V. (1976). *Phys. Rev.* A **13**, 1466.

Asaad, W. N., and Burhop, E. H. S. (1958). *Proc. Phys. Soc.* **71**, 369.

Bacskay, G. B., Bryant, G., and Hush, N. S. (1986). *Int. J. Quant. Chem.* **30** (in press).

Bernheim, R. A., Gold, L. P., and Tipton, T. (1983). *J. Chem. Phys.* **78**, 3635.

Bhatia, A. K., Temkin, A., and Silver, A. (1975). *Phys. Rev.* A **12**, 2044.

Chang, T. N., and Poe, R. T. (1975). *Phys. Rev.* A **11**, 191.

Cooper, J. W. (1974). *Phys. Rev.* A **9**, 2236.

Cooper, J., and Zare, R. N. (1969). *In* 'Lectures in Theoretical Physics', Vol. 11C (Eds S. Geltman, K. T. Manhanthappa and W. E. Brittin) (Gordon and Breach: New York).

Davenport, J. W., Cosgrove, G. J., and Zangwill, A. (1983). *J. Chem. Phys.* **78**, 1095.

de Alti, G., Decleava, P., and Lisini, A. (1983). *Chem. Phys.* **80**, 229.

Douglas, T. B., Epstein, L. F., Dever, J. L., and Howland, W. H. (1955). *J. Am. Chem. Soc.* **77**, 2144.

Eisel, O., Demtröder, W., Müller, W., and Botschwina, P. (1983). *Chem. Phys.* **80**, 329.

Faegri, K., and Manne, R. (1976). *Mol. Phys.* **31**, 1037.

Fano, U., and Lichten, W. (1965). *Phys. Rev. Lett.* **14**, 627.

Gerard, P. (1984). Doctorate Thesis, Université de Paris-Sud.

Harris, S. E. (1980). *Opt. Lett.* **5**, 1.

Hessel, M. M., and Vidal, C. R. (1979). *J. Chem. Phys.* **70**, 4439.

Howat, G., Åberg, T., and Goscinski, O. (1978). *J. Phys.* B **11**, 1575.

Huber, K. P., and Herzberg, G. (1979). 'Constants of Diatomic Molecules' (Van Nostrand Reinhold: New York).

Huzinaga, S. (1965). *J. Chem. Phys.* **42**, 1293.

Huzinaga, S., McWilliams, D., and Domsky, B. (1971). *J. Chem. Phys.* **54**, 2283.

Hyman, H. A., and Mani, S. A. (1977). *Opt. Commun.* **20**, 209.

Konowalow, D. D., and Fish, J. L. (1984). *Chem. Phys.* **84**, 463.

Krummacher, S., Schmidt, V., Bizau, J. M., Ederer, D. L., Dhez, P., and Wuilleumier, F. (1982). *J. Phys.* B **51**, 4363.

Larkins, F. P. (1972). *J. Phys.* B **5**, 571.

Larkins, F. P., Adeney, P. D., and Dyall, K. G. (1981). *J. Electron Spectrosc.* **22**, 141.
McDowell, M. R. C., and Chang, E. S. (1969). *Mon. Not. R. Astron. Soc.* **142**, 465.
Manson, S. T. (1976). *Adv. Electron. Electron Phys.* **41**, 73.
Richards, J. A., and Larkins, F. P. (1983). *J. Electron Spectrosc. Relat. Phenom.* **32**, 193.
Richards, J. A., and Larkins, F. P. (1984). *J. Phys.* B **17**, 1015.
Richards, J. A., and Larkins, F. P. (1986). *J. Phys.* B **19**, 1945.
Roothaan, C. C. J. (1960). *Rev. Mod. Phys.* **32**, 179.
Schmidt-Mink, I., Müller, W., and Meyer, W. (1985). *Chem. Phys.* **92**, 263.
Schwarz, W. H. E., Butscher, W., Ederer, D. L., Lucatorto, T. B., Ziegenbein, B., Mehlorn, W., and Prömpeler, J. (1978). *J. Phys.* B **11**, 591.
Siegbahn, H., Asplund, L., and Kelfve, P. (1975). *Chem. Phys. Lett.* **35**, 330.
Stull, D. R., and Prophet, H. (Eds) (1977). 'JANAF Thermochemical Tables', National Standard Reference Data Series (National Bureau of Standards: Washington, D.C.).
Sukumar, C. V., and Kulander, K. C. (1978). *J. Phys.* B **24**, 4155.
Tiwari, P., Hashim, M. A., Ojha, S. P., and Rustgi, O. P. (1977). *Can. J. Phys.* **55**, 972.
Tully, J. C., Berry, R. S., and Dalton, B. J. (1968). *Phys. Rev.* **176**, 95.
Wentzel, G. (1927). *Z. Phys.* **43**, 524.
Yang, C. N. (1948). *Phys. Rev.* **74**, 764.
Ziem, P., Bruch, R., and Stolterfoht, N. (1975). *J. Phys.* B **8**, L480.

Manuscript received 12 March, accepted 10 June 1986